10

Plasma flame sustained by microwave and burning hydrocarbon fuel: Its applications

Yongcheol Hong[1] and Han Sup Uhm[2]
[1]*National Fusion Research Institute*
[2]*Kwangwoon University*
[1,2]*Korea*

1. Introduction

Thermal plasma torches have been developed for various industrial applications. Industries require them to be high power, contaminant-free, low-maintenance, low-cost, and large-volume. Principally, the plasma torch is a device to produce an arc plasma column between two electrodes. There are several kinds of plasma torches, including dc arc torch, induction torch, and high-frequency capacitive torch. The dc arc torch is operated by the dc electric field between two electrodes at a severe environment of high arc current in the range from several tens to thousands of amperes. Therefore, their electrodes are replaced often due to their limited lifetime, in particular an oxidative environment. Almost all radio frequency torches are inductively coupled discharges. Their typical thermal efficiencies (% of power effectively dissipated in the plasma forming gas) are in the range of 40-50% (Fauchais & Vardelle, 1997). These conventional torches also have a small volume of plasma, high operational cost and require many expensive additional systems for operation. Although the conventional plasma torches are used in many industrial applications, the wide acceptance of these processes is limited by economic, competitive, reliability, and other concerns. From the reason above-mentioned, they may not be useful in environmental applications.

In order to overcome problems related with the conventional plasma torch, an electrodeless microwave plasma torch at atmospheric pressure was developed (Hong et al., 2003; Kim et al., 2003). Microwave plasmas operated at the atmospheric pressure, especially waveguide-based plasma, have been subject of increased attention during the last decade (Margot, 2001; Moisan et al., 2001). Such an interest comes from their potential and actual use in various applications, including excitation sources for elemental analysis, lighting, and purification or remediation of gas effluents detrimental to the environment (Hartz et al., 1998; Woskov & Haddi, 1999). The microwave plasma torch can easily be made by modifying typical household microwave ovens as inexpensive method (Kim et al., 2003). Therefore, the microwave plasma torch is simple, compact and economical. Furthermore, in previous works, the microwave plasma torch has been investigated in various applications such as the abatement of CF_4, NF_3 and SF_6, the elimination of chemical and biological warfare agents, and synthesis of carbon nanotube, titanium dioxide, titanium nitride, and zinc oxide (Hong et al., 2004; Kim et al., 2007). Although the microwave plasma torch in air discharge

provides high plasma density and high gas temperature in inexpensive ways (Green, 2001), the plasma volume and temperature of the microwave plasma torch decrease drastically outside the discharge tube, thereby limiting its capability of bulk treatment of waste. For example, the gas flow rates in the treatment experiments of CF_4 and phosgene were only tens of liters per minute (lpm), although high destruction and removal efficiency more than 96% had been accomplished (Hong et al., 2003; Hong et al., 2005). In this context, plasma flames made of a microwave plasma and a fuel burning flame have been developed for producing an enlarged high-temperature plasma flame by injecting a hydrocarbon fuel into the microwave plasma torch. The complete combustion of a hydrocarbon fuel in the microwave plasma torch causes the increase of plasma flame volume, high temperature zone, and residence time of target materials in high temperature zone.

There are many experimental investigations related to the fuel combustion using arc plasma torch and microwave. Since the experimental research in the 1970s (Weinberg et al., 1978), studies on plasma torch igniters have been extensively conducted. The advantages of a plasma torch in combustion are its role as a source of a radical pool and high temperature. Recently, Takita et al. showed that a considerable increase in burning velocity by addition of radicals occurred only in the case when the mixture temperature was high and the mixture included a large number of radicals (Takita, et al., 2001). Also, Masuya *et al*. investigated the ignition of H_2, H_2/N_2, H_2/air, and O_2/N_2 in high-temperature airflow by an arc torch (Masuya et al., 2002). The effects of microwave radiation on combustion were experimentally investigated by many researchers. For instance, Ogawa et al. investigated the influence of microwaves on CH_4/air laminar flames in a cavity resonator excited at 2.45 GHz by measuring the burned-gas temperature, brightness, and electron temperature (Ogawa et al., 1998). Finally, it is concluded that the combustion enhancement by microwave is due to the microwave heating of the bulk gases in the flame zone, and thus yielding a greater flame temperature. Therefore, the microwave plasma burning system can provide a near perfect combustion of a hydrocarbon fuel gas with air or oxygen gas due to the high-temperature plasma and a large quantity of radicals in the microwave plasma. For instance, in destructing fluorinated compound gases (FCs) using a microwave plasma torch (Hong et al., 2003), the impact process of electrons dissociates or ionizes FC molecules, and other plasma constituents convert into benign or more treatable products by injecting into the center part of the microwave plasma torch flame sustained from any gas mixture. However, the microwave torch abated the contaminants only in 10-20 lpm nitrogen gas contaminated by CF_4, SF_6, and NF_3 gases. The reason for the abatement limitation of the microwave plasma torch is due to the small volume of the torch plasma and the short residence time of contaminants in the reactor. Actually, the volume of the plasma flame sustained by the microwave plasma and burning hydrocarbon fuel is much larger than that of the microwave plasma torch. Therefore, the large-volume, high temperature plasma flame is expected to overcome the abatement limitation at high flow rate.

This chapter contributes the combustion enhancement of a hydrocarbon fuel augmented by the microwave plasma torch. Also, this chapter describes the configuration of plasma flame generator made of a microwave plasma and a fuel-burning flame, investigates physical properties containing its temperature and optical emission, and lastly shows the experimental results in abating fluorinated compound gases, decontaminating chemical and biological warfare agents, and eliminating odorous chemical agents.

2. Microwave plasma torch

Figure 1 displays a schematic configuration of the atmospheric pressure microwave plasma system. The design and operation of the atmospheric microwave plasma torch are briefly summarized here for completeness, although they have been reported in detail in previous articles (Hong et al., 2003; Kim et al., 2003). It is comprised of the 2.45 GHz microwave generator, WR-340 waveguide components, including an isolator, a directional coupler, a 3-stub tuner, and a microwave plasma torch as a field applicator. The WR-340 waveguide (86 mm × 43 mm) used in the microwave plasma torch was tapered to a reduced cross-section of 86 mm × 20 mm. In the unloaded waveguide without plasma, the reduction of the waveguide height provides an increase in the electric field strength even with the same microwave power. Due to the Poynting theorem, we get about a $\sqrt{2}$ times higher electric field strength in the plasma torch region. The discharge tube was inserted vertically, perpendicular to the wide wall of the waveguide. The discharge tube was located at a 1/4 wavelength away from the shorted end of the waveguide. The highest-intensity electric field occurs at this location confirmed by a high frequency structure simulator code (Kim et al., 2003). The microwave radiation generated from magnetron passes through the 3-stub tuner, is guided through the tapered waveguide, and enters the discharge tube made of fused silica. The center axis of the discharge tube with an outer diameter of 30 mm is located one-quarter wavelength from the shorted end of the waveguide. The tube penetrates through the wide waveguide walls, as shown in Fig. 1. The igniters not shown in Fig. 1 with their terminal electrodes inside the discharge tube initiate the plasma. The plasma generated inside the discharge tube is stabilized by a swirl gas, which enters the discharge tube sideways, creating a vortex flow (Gutsol et al., 1998) in the tube. The impedance of the plasma and the field applicator to the characteristic impedance of the WR-340 waveguide were matched by tuning the 3-stub tuner. The reflected power adjusted by the 3-stub tuner is almost zero. Even with all the tuning stubs completely withdrawn, reflected power is typically less than 10% of the forward power (Hong et al., 2003). The forward and reflected powers are monitored by the directional coupler.

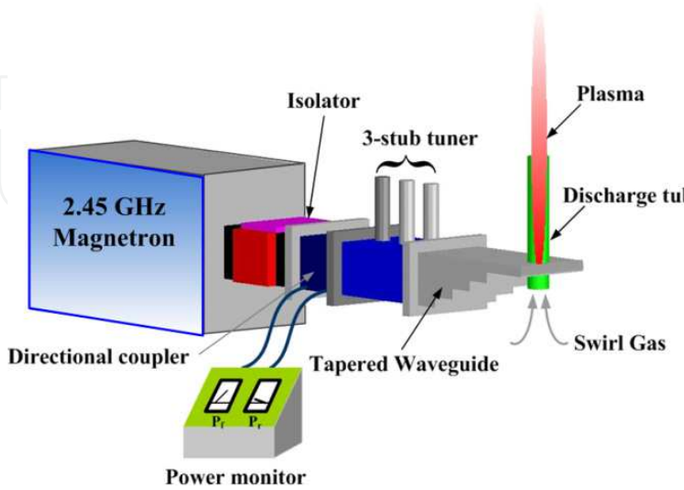

Fig. 1. Schematic presentation of the 2.45 GHz microwave system components and the microwave plasma torch.

A number of experimental results in atmospheric microwave plasmas have been reported (Green et al., 2001; Moon et al., 2002). For example, Green et al. measured the torch flame temperature inside a discharge tube by making use of the Fe I emission lines in the 370-377 nm range (Green et al., 2001). The microwave plasma torch is similar or almost same with ours. The temperature profiles are almost flat out to the largest measurable plasma radius of 10 mm with a maximum value of 6550 ± 350 K on axis at an air of 28 lpm and 1.4 kW power. The flame temperature at the 10 mm radius is still 80% of its value on axis. Generally, the plasma column length in the microwave plasma torch depends on the amount of swirl gas. In previous literature (Kim et al., 2003), the plasma column length was about 20-30 cm for 1 kW microwave power, for a discharge tube with 27 mm inner diameter and for 20 lpm of air swirl gas. The plasma column length was reduced to 10 cm when the swirl gas increased from 20 to 80 lpm. The microwave plasma torch can be operated in various gases. In this context, Figs. 2(a)-(f) reveal the microwave discharge plasmas in 10 lpm argon, 1 lpm argon, 10 lpm helium, 10 lpm nitrogen, 10 lpm air, and mixture of 5 lpm nitrogen and 10 lpm helium, respectively.

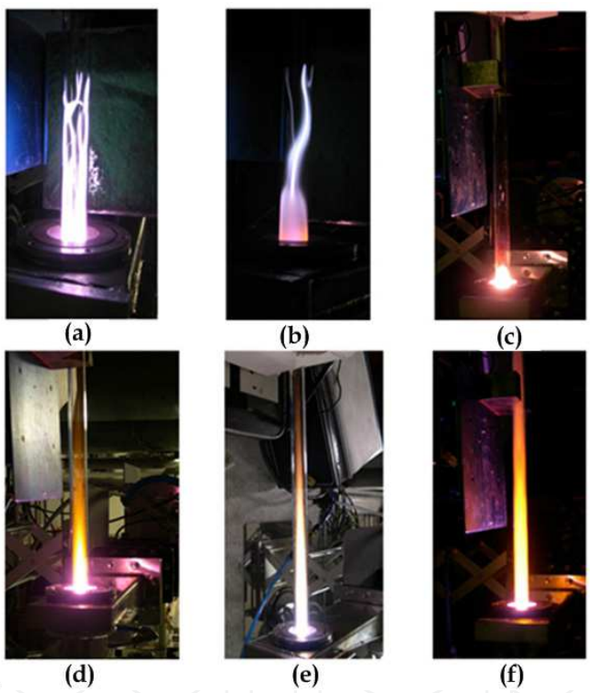

Fig. 2. Various atmospheric pressure microwave plasmas at (a) 10 lpm argon, (b) 1 lpm argon, (c) 10 lpm helium, (d) 10 lpm nitrogen, (e) 10 lpm air, and (f) mixture of 5 lpm nitrogen and 10 lpm helium. Then, the applied microwave power is approximately 1 kW.

3. Plasma flame generator

3.1 Arrangement of plasma flame generator

Figure 3(a) shows the schematic view for the plasma flame generator made of the microwave plasma and a fuel-burning flame. The main parts of experimental configuration for the plasma flame generator, as shown schematically in Fig. 3(a), consist of the microwave

plasma torch, a fuel-injector, and a plasma flame exit. Air, oxygen or a mixture of air and oxygen can be used as a swirl gas. Therefore, the swirl gas provides atomic oxygen and molecular singlet oxygen of high-density (Lai et al., 2005) for near perfect combustion of hydrocarbon fuels, which is sprayed from the fuel injector in Fig. 3(a). The fuel injector, which is a typical fuel nozzle used in home-boilers, is equipped with the stainless steel tube and provides fuel for plasma. The injector is installed contiguously to the upper side of the waveguide, as shown in Fig. 3(a). The inner diameter of stainless steel tube has the same inner size as the discharge tube and is installed on the tapered waveguide to sustain a steady vortex flow of the swirl gas. The hydrocarbon fuel injected into plasma mixes with the swirl gas (air or oxygen) and extends the plasma flame to the open air, evaporating instantaneously and breaking down the molecular structure by energetic electrons and high temperature. The temperatures at different positions of the plasma flame were measured by a thermocouple of *R* type. The marks L_0 ~ L_{15} in Fig. 3(a) indicate the temperature-measurement points. For example, the mark L_6 represents a measurement point 6 cm away from the plasma flame exit. The mark $L_{-1.5}$ is the position corresponding to a measurement point 1.5 cm away the direction of the wide-wall waveguide. Fig. 3(b) is the cross-sectional view of swirl generator marked with dotted line in Fig. 3(a). The swirl gases are injected towards tangential direction through four tangential holes. The holes for the swirl gases are inclined towards axial direction by 30° .

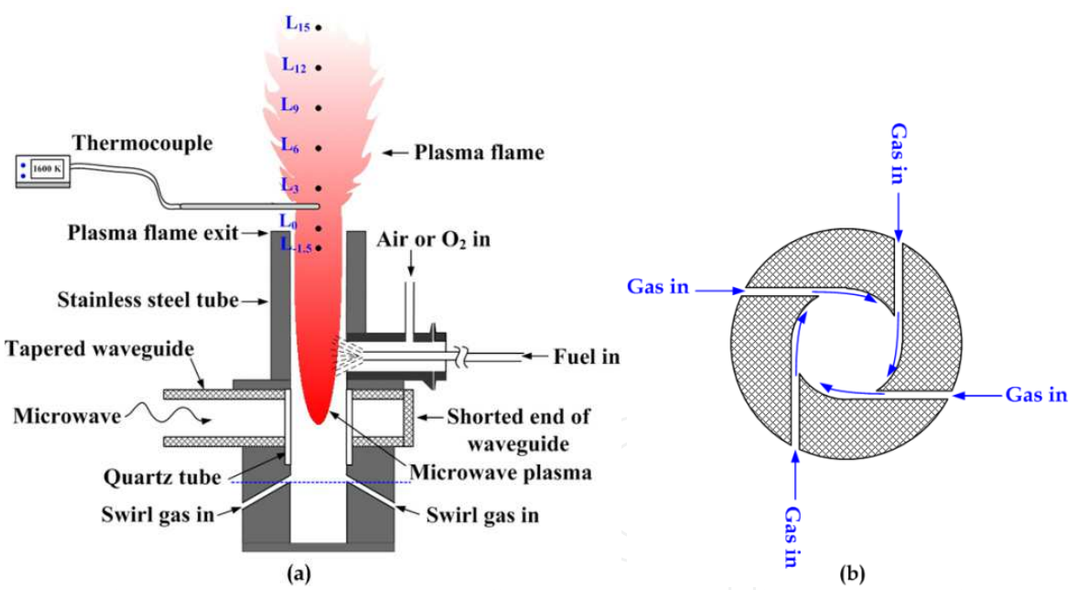

Fig. 3. (a) Schematic view shows a plasma flame generator with the microwave plasma torch. The fuel injector was installed adjacent to the upper side of the waveguide. (b) Cross-sectional view displays a swirl gas generator with four tangential holes for the dotted line in (a)

3.2 Temperature profile of plasma flames

3.2.1 Plasma flame from kerosene

Generally, flames already contain a weakly ionized plasma with typical density greater than 10^{10} ions/cm^3. For example, the oxidation of methanol by atomic oxygen is 10 million times

faster than that by oxygen molecules at the gas temperature of 1300 K (Uhm, 1999). If so, as mentioned earlier, because the microwave plasma torch has high plasma density of ~10^{13}/cm^3 in air discharge and high temperature of about 6500 K at the center axis (Green et al., 2001), we expect that the microwave plasma torch can accomplish near perfect combustion of fuel. In this regard, Figs. 4(a) and (b) show the microwave plasma-burner flames before and after the fuel injection at the applied microwave power of 1.5 kW, respectively. In Fig. 4(a) and (b), a mixture of 50 lpm air and 10 lpm oxygen as a swirl gas was injected into the microwave plasma torch, while 50 lpm air as a swirl gas and 10 lpm oxygen with a fuel through the fuel injector were injected in Fig. 4(c). Figure 4(a) is a picture of the plasma torch flame without fuel injection. The flame was not expanded to the exit of the stainless steel tube of 10 cm in length. However, as shown in Fig. 4(b) and (c), the burner flame shot out through the exit of the stainless steel tube when 0.025 lpm kerosene was injected as a fuel into the microwave plasma torch. The burner flame diameter and length from the flame exit were about 8 cm and 40 cm, respectively. As a matter of fact, the fuel injector in this work was installed just above the waveguide and was 2 cm away from the waveguide excitation region, as shown in Fig. 3(a). When 10 lpm oxygen gas was added to the microwave plasma torch, not shown in Fig. 4, it was observed that the plasma flame color changed from a yellowish white to a bluish white, implying the phenomenon of near perfect combustion.

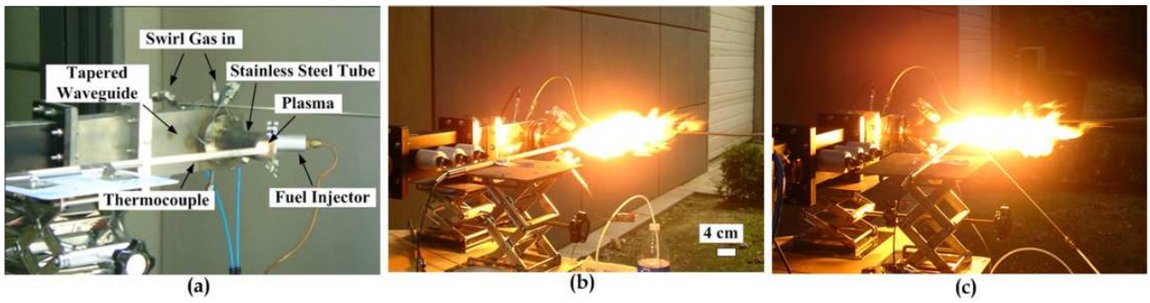

Fig. 4. Microwave plasma-burner flames before (a) and after (b and c) a fuel injection at the applied microwave power of 1.5 kW. A mixture of 50 lpm air and 10 lpm oxygen as a swirl gas was injected into the microwave plasma torch in (a) and (b), while 50 lpm air as a swirl gas and 10 lpm oxygen with a fuel through the fuel injector were injected in (c) (Hong et al., 2006).

The temperature of the microwave plasma torch flame at the center of the flame exit (mark L_0 in Fig. 3) measured by a thermocouple was only 550 K, when 60 lpm air as a swirl gas was injected. However, the temperature of the burner flame with the addition of 0.025 lpm kerosene drastically increased to about 1380 K. Moreover, the temperature of the burner flame with the addition of 0.025 lpm kerosene and 10 lpm oxygen gas drastically increased to about 1700 K. Temperature distributions along the radial and axial directions at different kerosene flow rates were measured with the addition of oxygen. Figure 5(a) shows the radial temperature profiles at marks L_0, L_3, and L_6 when a mixture of 40 lpm air and 20 lpm oxygen as a swirl gas and 0.025 lpm kerosene were injected. The length of the flame was about 30 cm. Each line marked by the rectangles, circles, and triangles indicates the radial temperature distribution at 0, 3, and 6 cm from the stainless steel tube. In comparison with the temperature distributions at L_3 and L_6, the distribution at L_0 decreases more drastically

owing to the small inner diameter of the exit. Generally speaking, the volume of the burner flame decreases as oxygen flow rate increases, while the flame temperature at the center axis increases. As shown in Fig. 5(a), temperatures at L_0, L_3, and L_6 distribute from 1750 to 1850 K, revealing approximately uniform temperature-distribution in the axial direction. Figure 5(b) presents the axial temperature profiles at different kerosene flow rates, when a mixture of 50 lpm air and 10 lpm oxygen as a swirl gas was injected. Each line marked by the rectangles, circles, and triangles indicates the axial temperature profiles at kerosene flow rates of 0.031, 0.025, 0.019 lpm, starting from the stainless steel tube. The fuel injectors of 0.031 and 0.025 lpm spray the fuel in a shape of a conic shell with 80° spraying angle. The injector of 0.019 lpm sprays the fuel in the shape of a solid cone with 60° spraying angle. As shown in Fig. 5(b), it is observed that the trends of the temperature profiles at axial positions 0 and 3 cm depend on the type and angle of fuel injection. The difference of the mixture of swirl gas and fuel in the stainless steel tube causes different trend in temperature profiles. Generally speaking, flame temperature and volume increase as the kerosene flow rate increases.

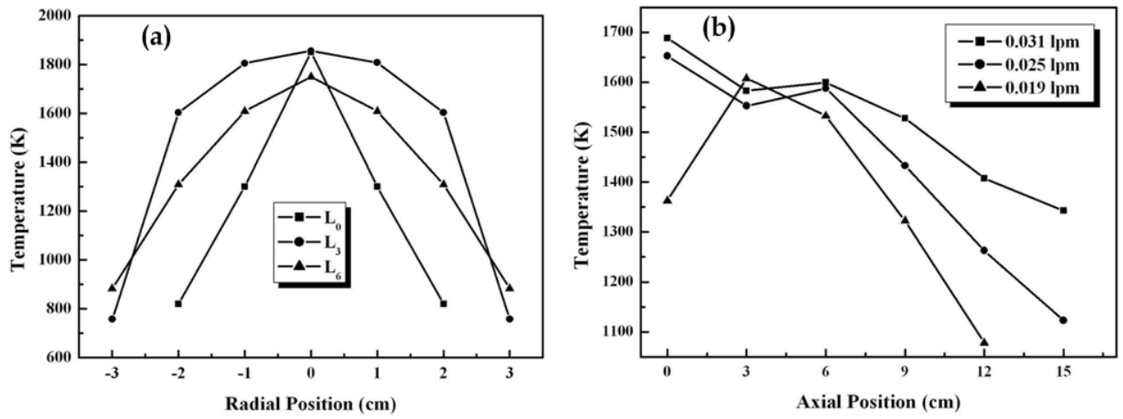

Fig. 5. Radial temperature profile (a) when a mixture of 40 lpm air and 20 lpm oxygen as a swirl gas and 0.025 lpm kerosene were injected into the microwave plasma torch and axial temperature profile (b) at kerosene flow rates of 0.031, 0.025, and 0.019 lpm when a mixture of 40 lpm air and 20 lpm oxygen as a swirl gas was injected (Hong et al., 2006).

3.2.2 Plasma flame from diesel

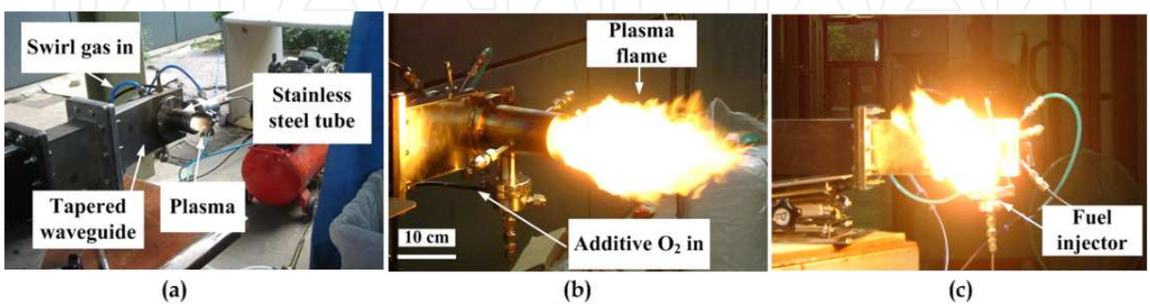

Fig. 6. Diesel microwave plasma-burner flames (a) before and (b and c) after a fuel injection at the applied microwave power of 1.2 kW. 50 lpm air as a swirl gas and 10 lpm oxygen with 0.019 lpm diesel through the fuel injector were injected, where (c) is a front view of picture (b) (Hong & Uhm, 2006).

In Fig. 6, the plasma flames before and after the injection of diesel fuel were compared. Similar to the kerosene microwave plasma burner reported in the previous work (Hong, et al., 2006), the diesel microwave plasma flame also shows that the volume is more than 50 times that of the torch plasma, burning diesel fuel instantaneously. Figure 6(a) is a picture of the microwave plasma torch flame operated at 1.2 kW microwave power, 50 lpm air as a swirl gas, and 10 lpm oxygen through the fuel injector without diesel. Figure 6(b) is a picture of the plasma flame generated by 50 lpm air as a swirl gas and 10 lpm oxygen with 0.019 lpm diesel injection through the fuel injector. Figure 6(c) is a front view of Fig. 3(b). While the torch flame in Fig. 6(a) is weakly expanded to the exit of the stainless steel tube of about 10 cm in length, the burner flames shot out through the exit of the stainless steel tube when 0.019 lpm diesel was injected as a fuel into the microwave plasma torch, as shown in Figs. 6(b) and (c). The plasma flame diameter and length from the flame exit were about 8 cm and 30 cm, respectively. The liquid diesel can evaporate instantaneously, breaking down the molecular structure by the microwave plasma column with high gas temperature, and burn immediately with oxygen. The fuel injector in this work was installed just above the waveguide and was approximately 2 cm away from the waveguide excitation region, as shown in Fig. 3(a). When 20 lpm oxygen gas with 0.019 lpm diesel was additionally injected into the microwave plasma torch, not shown in Fig. 6, it was observed that the plasma flame color changed from a yellowish white to a bluish white, indicating a high temperature at oxygen injection. In this context, we measured the gas temperature of the diesel microwave plasma flame in terms of oxygen content.

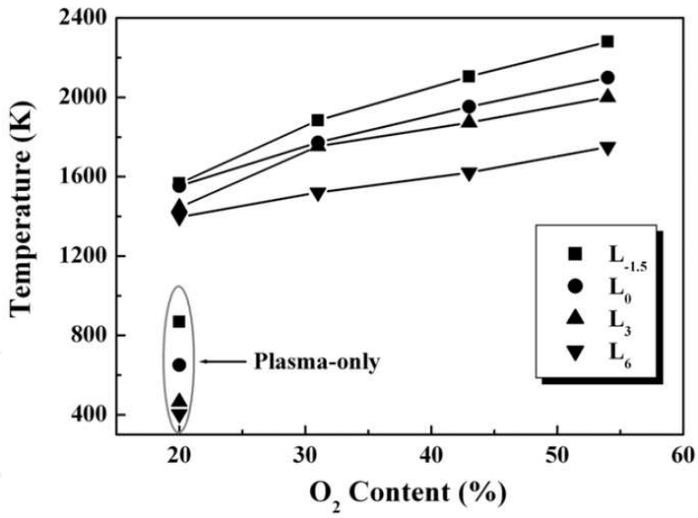

Fig. 7. Axial temperature profiles of the plasma flame in terms of O_2 content (%) at 0.019 lpm diesel. Total flow rate of mixture of air and O_2 was 70 lpm and the applied microwave power was 1.2 kW. The mixture was injected as a swirl gas (Hong & Uhm, 2006).

Figure 7 exhibits the gas temperature profiles of the diesel microwave plasma flames measured axially by a thermocouple in terms of oxygen content (%) at $L_{-0.5}$, L_0, L_3, and L_6 in Fig. 3(a). The total flow rate of the mixture composed of air and oxygen was fixed at 70 lpm and the mixture was injected into the microwave plasma torch as a swirl gas. For example, O_2 content of 54% represents the mixture composed of 40 lpm air and 30 lpm O_2. In the case

of 20% O_2, while the gas temperatures of the microwave plasma torch flame at four measurement positions distribute in the range of 400-850 K, the gas temperatures of the plasma flame with 0.019 lpm diesel are in the range of 1400-1600 K. Moreover, when O_2 content at $L_{-1.5}$ position increases from 20% to 54%, the gas temperature significantly increases from 1580 K to 2210 K. In general, the diesel plasma flame shows similar properties with the kerosene plasma flame such as Fig. 4.

3.2.3 Plasma flame from methane

Figure 8(a) shows the microwave plasma torch flame at applied power of 1.2 kW when 60 lpm air as a swirl gas was injected. As shown in Fig. 8(b), however, once CH_4 (10 lpm in this test) as a hydrocarbon fuel is injected into the microwave plasma torch through the fuel injector in Fig. 3(a), volume of the CH_4 plasma burner flame significantly increases, emitting milky white lights. Fig. 8(c) is the CH_4 flame picture without the microwave plasma. Unlike Fig. 8(b), Fig. 8(c) shows the flame with light blue color. The flame temperature of Fig. 8(b) and (c) at the point of L_0 in Fig. 3(a) is ~1590 K and 1250 K, and the visual flame length of Fig. 2(b) and (c) is 18 cm and 11 cm, respectively. From another experiment result of CH_4 microwave plasma burner not shown in this chapter, it is identified that CH_4 injection rate up to 30 lpm (near 0.36 g/s) is reasonable at 1.2 kW microwave plasma torch and stoichiometric fuel/air mixture. For practical application such as power plant, a microwave plasma torch with 915 MHz or 896 MHz microwave system or multiple microwave plasma torches may be suitable for obtaining high power.

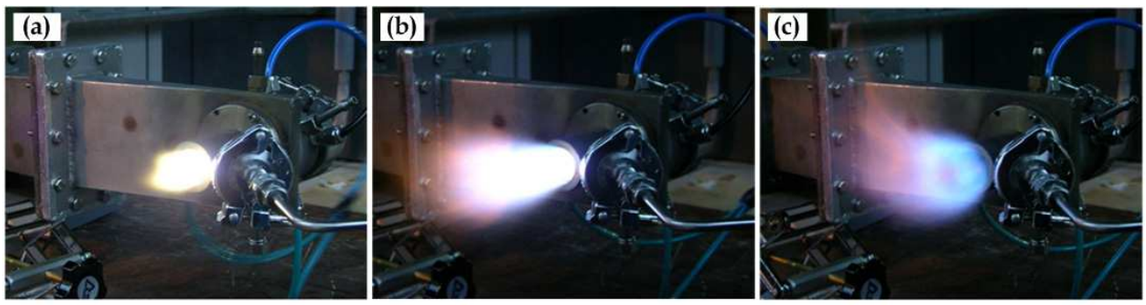

Fig. 8. Plasma-burner with (a) microwave plasma only, (b) microwave plasma + CH_4 injected at 10 lpm and (c) CH_4 flame only (Bang et al., 2006).

In this regard, we measured temperatures of the CH_4 microwave plasma burner flame at different positions presented in Fig. 3(a). The rectangular marks in Fig. 9(a) represent the axial temperature profile of the plasma burner flame at marks L_0-L_{15} when 60 lpm air as a swirl gas, and a mixture of 10 lpm CH_4 and 40 lpm air through the fuel injector were injected the microwave plasma torch. Therefore, the value of mixture ratio of air/CH_4 is 10 : 1. The temperature of the microwave plasma torch flame at the center of the flame exit (mark L_0 in Fig. 1) was only 600 K without CH_4. As shown in Fig. 9 (a), the temperature of the plasma burner flame increased to about 1890 K when 10 lpm CH_4 was injected. And then the visual length of the burner flame was about 24 cm. It is well-known that the adiabatic flame temperature of a CH_4/air flame is about 2222 K. 1890 K in this test is flame temperature measured at the point away 5 cm from the fuel injector in Fig. 1. Therefore, the burner flame temperature near a region of fuel injection may be as high as that of CH_4/air flame in

adiabatic condition. The circular marks in Fig. 9(b) indicate the axial temperature profile of the burner flame when 40 lpm air as a swirl gas, and a mixture of 10 lpm CH_4 and 60 lpm air was injected through the fuel injector. With 10 lpm CH_4, temperature of the burner flame increased from 600 K to 1680 K. And then the visual length of the burner flame in Fig. 9(b) was approximately 30 cm. Compared Fig. 9(a) with (b), the temperature profile in Fig. 9(a) falls rapidly at axial position of 6 cm, whereas the temperatures in Fig. 9(b) reduce gently along with axial direction. In this context, Fig. 9 implies that the temperature and length of the burner flame can be controlled by injection way or mixing rate of air and fuel. In general, it is recognized that the use of a thermocouple for measurement of flame temperatures may encounter some problems. Also, flames already contain a weakly ionized plasma with typical density greater than 10^{10} ions/cm^3 (Uhm, 1999). However, the thermocouple used in this test is perfectly covered with alumina (Al_2O_3). So plasma impacts in temperature measurements may be neglected.

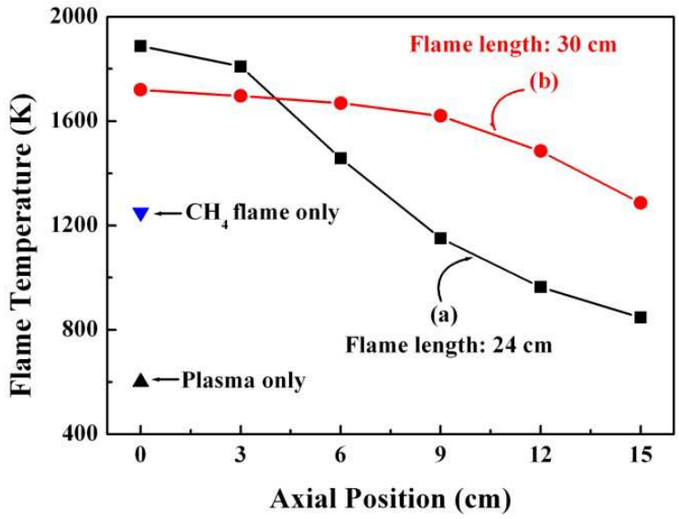

Fig. 9. Axial temperature profiles of the CH_4 augmented microwave plasma burner measured at positions L_0-L_{15} as denoted in Fig. 3(a). (a) 60 lpm swirl air + mixture of 10 lpm CH_4 and 40 lpm air. (b) 40 lpm swirl air + mixture of 10 lpm CH_4 and 60 lpm air (Bang, et al., 2006)

Figure 10 shows the radial temperature profile of the CH_4 augmented microwave plasma burner at marks L_0 in Fig. 1. The rectangular marks in Fig. 10(a) indicate the radial temperature profile of the burner flame when 60 lpm air as a swirl gas, and a mixture of 10 lpm CH_4 and 40 lpm air through the fuel injector were injected the microwave plasma torch. As shown in Fig. 10(a), the temperature of the burner flame decreased to about 1180 K, rapidly. The circular marks in Fig. 10 (b) indicate the radial temperature profile of the burner flame when 40 lpm air as a swirl gas, and a mixture of 10 lpm CH_4 and 60 lpm air through the fuel injector were injected the torch. The temperature of the burner flame decreased to about 1370 K, slowly. Figs. 9 and 10 showed the axial and radial temperature profiles in CH_4 augmented microwave plasma burner flame, respectively. The performance of CH_4 microwave plasma burner significantly depends on the physical and chemical properties of microwave plasma torch. The theoretical description of the microwave plasma torch is beyond the scope of the present study. However, one can refer the previous articles (Kim et

al., 2003; Margot, 2001; Moon et al., 2002) describing the atmospheric pressure microwave plasma torch.

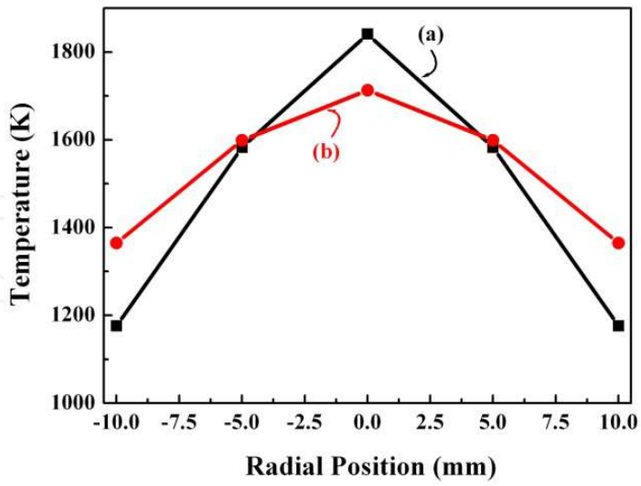

Fig. 10. Radial temperature profiles of the CH_4 augmented microwave plasma burner measured at position L_0 in Fig. 3(a). (a) 60 lpm swirl air + mixture of 10 lpm CH_4 and 40 lpm air. (b) 40 lpm swirl air + mixture of 10 lpm CH_4 and 60 lpm air (Bang et al., 2006).

The temperature profiles in Figs. 9 and 10 were changed with addition of the same CH_4 quantity at different swirl air flow rates and air flow rates through the injector. When a swirl air flow rate is more than that through the injector, the vortex flows inside the stainless steel tube in Fig. 3(a) can survive against air flow through the injector, increasing the combustion time of CH_4, confining the CH_4 flames axially, and thus increasing the temperature at L_0 point. On the other hand, when a swirl air flow rate is less than that through the injector, an air flow through the injector can suppress vortex flow by swirl air injection and increase axial flow velocity and flame length. Therefore, even though the same CH_4 flow rate is injected, each temperature profile in Figs. 9 and 10 can be changed due to different gas injection methods.

3.3 Simple description of atomic oxygen density in plasma flames

Principally, a discharge plasma and a high temperature environment generate many chemically active radicals. For example, oxygen atoms can be generated by the plasma and thermal dissociations of oxygen molecules, i.e., $O_2 \rightarrow O + O$. Plasma dissociation includes dissociative recombination of molecular oxygen ions, electron impact dissociation of oxygen molecules, and dissociative attachment of oxygen negative ions (Uhm, 1999). Thermal dissociation of oxygen molecules has reaction constant (Hong & Uhm, 2006) $k = 2.7 \times 10^{11} (T_R/T_P)^2 \exp(-59429/T_P)$ s^{-1}, where T_R and T_P represent room and plasma flame temperature, respectively, in units of Kelvin. The oxygen atoms recombine with recombination coefficient $\alpha = 2.3 \times 10^{-14} (T_R/T_P)^2$ cm^3s^{-1}, forming oxygen molecules (Hong & Uhm, 2006). The oxygen atom may also form ozone with oxygen molecule but ozone dissociates rapidly due to high plasma temperature. Therefore, ozone from the microwave plasma torch is not produced. The rate equation of oxygen atom density n_O is given by

$$\frac{dn_O}{dt} = 2kn_{O2} - \alpha n_O^2, \tag{1}$$

with the solution

$$n_O(t) = \sqrt{\frac{2kn_{O2}}{\alpha}} \tanh(\frac{t}{\eta}), \tag{2}$$

where $\eta = 1/\sqrt{2k\alpha n_{O2}}$, n_{O2} is the molecular oxygen density and the factor 2 in front of k represents 2 atoms from one molecular dissociation. For instance, the plasma flame temperatures from the fuel injection point to L_9 point in Fig. 3(a) range in T_P = 4000-1500 K (Hong, et al., 2006). The oxygen atom formation by the plasma may be significant, but it is difficult to find the plasma effects in the plasma flame. Neglecting the plasma effects and assuming T_P = 2000 K as an average value, we find η = 1.5 s and $n_O(t = \infty) = 1.3 \times 10^{15}/cm^3$ for $n_{O2} = 6 \times 10^{17}/cm^3$. Assuming the residence time t = 0.06 s in the stainless steel tube in Fig. 3(a) as a typical value, the oxygen atom density is calculated to be $n_O = 5.7 \times 10^{13}/cm^3$ from Eq. (2), which effectively combusts hydrocarbon fuels. The oxygen atom density increases drastically with the high plasma-flame temperature originated from the plasma torch.

3.4 Influence of microwave plasma in plasma flame

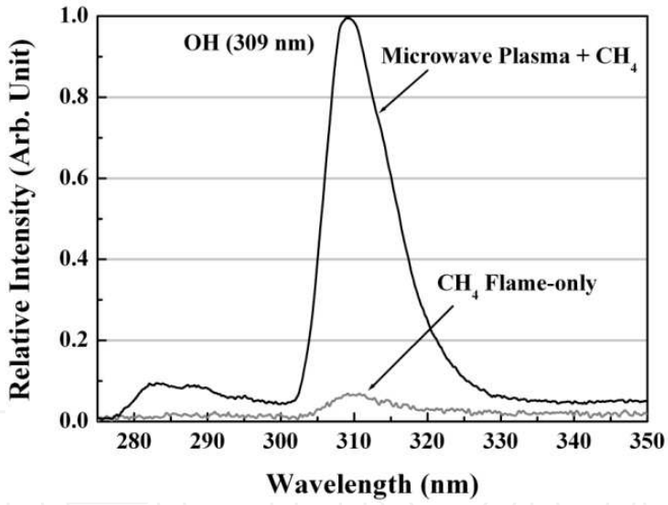

Fig. 11. Comparison of OH molecular intensities for CH_4 flame-only (gray) and plasma flame with CH_4 (black) (Hong & Uhm, 2006).

As above-mentioned, we compared CH_4 flame-only and the plasma flame with CH_4 by providing visual changes of flame color, flame lengths, and flame temperature by a thermocouple. These may be under the influence of the microwave plasma on the combustion flame. Here, we present the influence on the microwave plasma by observing hydroxyl (OH) molecules in an emission spectrum as a supporting data. OH molecular spectrum is necessarily observed in many kinds of flames and hot gases containing oxygen and hydrogen. In this sense, we compared the emission intensities of OH radical for CH_4 flame-only and CH_4 flame combined with the microwave plasma at L_0 point in Fig. 3(a). Experimental parameters correspond to the curve in Fig. 10(a). Figure 11 compares the

relative emission intensity of OH for CH_4 flame-only (gray line) and CH_4 flame combined with the microwave plasma (black line). Two OH emission intensities were normalized by the intensity of CH_4 flame combined with the microwave plasma. In general, perfect combustion of hydrocarbon fuels produces gaseous water and carbon dioxide as final resultant products. OH species are essential intermediates during the process of water production. OH emission intensity strongly depends on the density of atomic oxygen. According to the simple description for atomic oxygen mentioned earlier, the atomic oxygen density was estimated to be $n_O = 5.7 \times 10^{13}/cm^3$ from Eq. (2), which effectively combusts hydrocarbon fuels. Ultimately, oxygen atoms produced by the microwave plasma in air are very helpful for CH_4 combustion, thereby exhibiting strong OH intensity as shown in Fig. 11. On the contrary, OH intensity of CH_4 flame-only is very weak in the comparison with the plasma flame of CH_4 combustion. This difference of OH intensity reflects one of rotational temperature (T_{rot}) of OH molecules to be equal to the gas temperature of the flames (de Izarra, 2000).

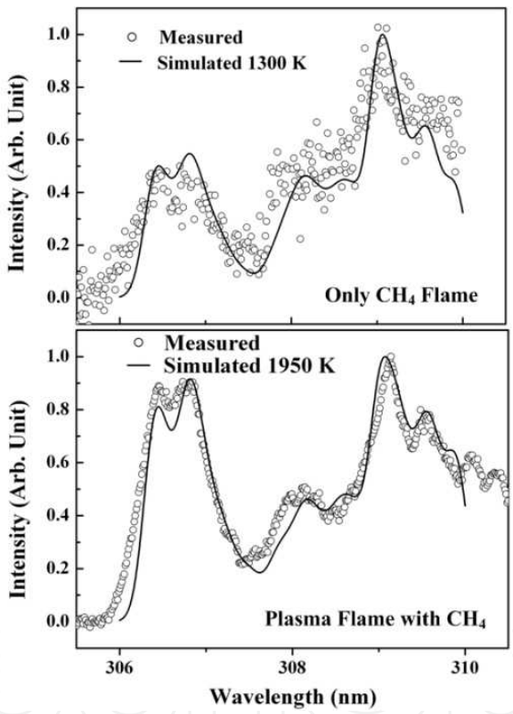

Fig. 12. Comparison of the measured data with the simulated OH spectrum for CH_4 flame-only and plasma flame with CH_4 yielding the rotational temperatures (T_{rot}) of 1300 K and 1950 K at L_0 point in Fig. 3(a) (Hong & Uhm, 2006).

In this context, Fig. 12 shows the unresolved OH molecular lines ($A\ ^2\Sigma^+,\ v=0 \rightarrow X\ ^2\Pi,\ v'=0$) observed in the wavelength of 306-310 nm with a spectral resolution of 0.35 nm. T_{rot} was determined in this study by comparing the simulated OH spectrum with the measured spectrum obtained at a relatively low spectral resolution. The method for obtaining simulated OH spectrum at a given temperature was provided in previous articles (de Izarra, 2000). The gas temperatures for CH_4 flame-only and the plasma flame with CH_4 in Fig. 12

are determined to be approximately 1300 K and 1950 K, respectively, showing the influence of the microwave plasma on CH_4 combustion.
A large, high-temperature plasma flame may be suitable for a bulk material treatment, in particular environmental application. As mentioned earlier, the microwave plasma torch in air discharge has small volume and its temperature decreases drastically in the axial direction. For example, CF_4, NF_3, and SF_6 abatement experiments conducted in our research group showed destruction efficiency more than 90% only in contaminant flow of 20 lpm (Hong et al, 2003). In order to overcome treatment limitation of the microwave plasma torch, a tool for an enlarged high-temperature plasma flames was designed. As shown in Fig. 9, the temperature difference between the CH_4 flame-only and the CH_4 microwave plasma burner flame is approximately 640 K. Therefore, the plasma constituents, such as atomic oxygen and molecular singlet oxygen, produced in the microwave plasma torch can be very helpful for hydrocarbon fuel combustion and may be useful in the thermal treatment processes.

4. Applications using plasma flames

4.1 Mass purification of contaminated air with chemical and biological warfare agents

The elimination experiment of any chemical warfare agent is almost impossible in an ordinary laboratory due to safety issues. Considering thus, the experimentalists customarily carry out a simulated experiment by making use of toluene gas. For this same reason, the biological warfare agents are not used in an ordinary laboratory (Hong, et al., 2004). The airborne biological warfare agents like microbes or bacteria are attached to organic or inorganic aerosols and are spread when aerosol particles float around. Consequently, the elimination of soot from a diesel engine as the simulated carrier aerosol of biological agents was carried out.
The reaction chamber for mass treatment of contaminated air was designed specially, providing the necessary residence time for the best decontamination effects. The detail explanation of the reaction chamber has been reported in previous article (Uhm et al., 2006). The toxic warfare agents contaminating air enters the inner compartment through slits from the outer compartment and are eliminated mainly by oxidation process exposed to the high-temperature plasma flame with abundant oxygen atoms in the inner compartment. The destruction model of the chemical and biological warfare agents can be expressed as (Hong et al., 2004)

$$\frac{X}{X_0} = \exp(-\frac{E}{\beta}), \tag{3}$$

where X represents the leftover concentration of the warfare agents after the plasma flame treatment and X_0 is the initial concentration before the treatment, E denotes the energy density (in units of joules per liter) deposited on the contaminated air by the plasma flame during the treatment and β represents the energy density required for bringing down the concentration to 1/e of its initial concentration; i.e. the energy density needed for 63 % decomposition. Designating R as the flow rate of the contaminated air, we note RE = constant for specified physical parameters of the decontamination system. In other words, the energy density E deposited by the plasma flame during the treatment is inversely proportional to the airflow rate R. Assuming that X_1 and X_2 correspond to the leftover concentrations for the flow rates R_1 and R_2, respectively, we find the relationship

$$\frac{R_1}{R_2} = \frac{\ln(X_0 / X_2)}{\ln(X_0 / X_1)}, \tag{4}$$

which relates the leftover concentration X to the airflow rate R. We can find the leftover concentration X_2 in terms of R_2 if we know the concentration X_1 in terms of R_1.

As an example, we used toluene (C_7H_8) as a simulated chemical warfare agent, and kerosene and methane were used as the hydrocarbon fuels. A liquid fuel is better than a gaseous fuel when pertaining to the instance of compactness and mobility. A suction fan supplied the contaminated air with evaporated toluene to the reaction chamber. The airflow rate was R = 5,000 lpm. 40 lpm of the compressed air was supplied to the swirl gas. The injection rates of the kerosene in this experiment were 1.15 kg/hr (≈ 0.3 gal/hr), 1.46 kg/hr and 1.87 kg/hr. The 0.3 gal/hr nozzle is the smallest fuel nozzle ever found. The methane flow rates were 5 lpm, 10 lpm, 15 lpm, 20 lpm and 30 lpm. The energy contained in kerosene and in methane are 10^7cal/kg and 9.52×10^6 cal/m^3, respectively. The fuel injection rate can be translated into watts. For example, a 1.15 kg/hr injection rate of kerosene is 13.3 kW and a 20 lpm injection rate of methane is also 13.3 kW. The energy density E in Eq. (3) can be calculated by making use of the fuel power and airflow rate. The microwave power was 1.4 kW and the initial toluene concentration was X_0 = 170 particulates per million (ppm). The kerosene injection rates 1.15 kg/hr, 1.46 kg/hr and 1.87 kg/hr with the microwave power of 1.4 kW correspond to the energy density E = 176.4 J/L, 219.4 J/L, and 276.3 J/L, respectively, for R = 5,000 lpm. The size of the reaction chamber used in the experiment was 22 cm diameter and 30 cm long. The compactness and lightweight of the decontamination system are the key issues for a quick and easy application in life-threatening situations. Therefore, the reaction chamber must be as small as possible for a specified airflow rate. The reaction chamber of 22 cm diameter and 30 cm length is good for the airflow rate of 5,000 lpm. The leftover concentration X of the toluene had been measured by making use of detector tubes from the GASTECH Company. The gas chromatography (GC) or the Fourier transform infrared (FTIR) can be used for more accurate data. In spite of this, those diagnostic tools may give completely wrong measurement values, because toluene is in liquid form at the room temperature of one atmospheric pressure. A sample leading to the diagnostic tools can easily be spoiled by toluene condensation. The measurement by detector tubes can be done at the flame exit of the reaction chamber without any delay or any interference. Therefore, the detector tube may reliably measure the leftover toluene, although the data may have a large error bar. Figure 13 shows the leftover toluene-concentration rate in terms of energy density for kerosene (closed square dots) and methane (open square dots) fuel injections. Each data point in Fig. 13 represents the average of 8 repeated measurements. The rectangular dots at E = 16.7 J/L represent toluene decomposition only by the microwave torch plasma with 1.4 kW. The typical error in the measurement as shown in the open square dot at E = 16.7 J/L of Fig. 13 is about 5 % associated with the detector tube. The error bars of most other data are smaller than the dot size in Fig. 13. The toluene curve in Fig. 13 for kerosene was obtained from Eq. (3) with the β-value that was least-squared fitted to the data points (closed square dots). The β-value of the toluene decomposition by the plasma flame is β = 84.76 J/L for kerosene, which is much less than β = 393 J/L by the pulse corona (Penetrante et al., 1997) and β = 173 J/L by the microwave plasma torch (Hong et al., 2004). The toluene curve in Fig. 13 for methane was obtained from Eq. (3) with the β-value that was least-squared fitted to the data points (open square dots). The β-value of the toluene decomposition by the plasma flame is β = 62.74 J/L for methane. Clearly, the toluene decomposition by the high-temperature plasma flame is far more efficient than that by the pulse corona or by the microwave torch. Furthermore, the present decomposition system is

very compact and light to be handy for various applications. The temperature of the reaction chamber wall and the exit gas is not hot due to a large amount of airflow. In fact, the outer wall of the reaction chamber only feels warm.

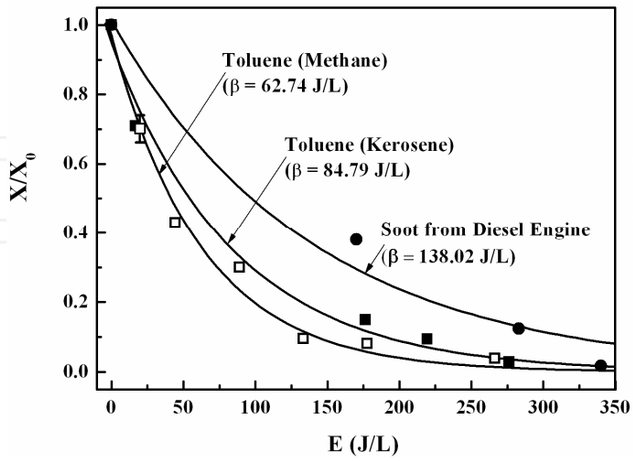

Fig. 13. Leftover toluene and soot concentrations in terms of the energy density *E*. The closed and open square dots represent measurement data for kerosene and methane injections, respectively, and the closed circular dots are the soot concentration data for methane injection (Uhm et al., 2006).

An elimination experiment of the airborne biological warfare agents is very difficult because of the complexity of detecting the agents before and after the plasma flame treatment. Spores of the biological warfare agents are usually attached to aerosol particles. The elimination of aerosol particles may indirectly show elimination of the airborne biological warfare agents. Elimination of soot from the diesel engine, which can be seen as airborne aerosol particles, was observed in the experiment. The burning kerosene may generate its own soot, which may interfere with the observation of the diesel engine soot, hence the gaseous fuel of methane was used in the experiment. The methane injection rate was 15 lpm, 25 lpm and 30 lpm in the soot elimination. The discharge gas from a 10,000cc bus diesel engine at 800 rpm was used as the contaminated air with soot. The airflow rate at the engine exit was 8,000 lpm, which is estimated to be 3,500 lpm at the end of the tail pipe due to the cooling of the ambient air. The energy density therefore was calculated by the methane injection into the airflow of 3,500 lpm. White filters captured soot from the discharge gas. A smoke meter from BOSCH, which determines opacity, measured the captured soot-amount in the filter. The remaining soot (closed circular dots) in relative to the untreated case is plotted in Fig. 13 in terms of the energy density for methane injected into plasma. The soot was almost completely eliminated at E = 340 J/L corresponding to the 30 lpm methane injection. The β-value of the soot elimination was determined by the least-squared-fitted to the experimental data (closed circular dots) in Fig. 13 and is given by β = 138.02 J/L. The plasma flame is an effective mean to eliminate the soot from the diesel engine. This means that the plasma flame may effectively eliminate airborne aerosol particles. Most of the aerosols are made of hydrocarbon materials, which can easily be oxidized at a high-temperature plasma flame with the temperature higher than 1000 degrees Celsius. The biological agents consisting of bacteria and virus may not survive as they go through the high-temperature plasma flame. Therefore, the plasma flame may effectively eliminate the

airborne biological warfare agents. A different experimental observation confirmed that the plasma flame of the kerosene or diesel injected into the torch plasma does not produce its own soot. In this context, the plasma flame can also be useful for the elimination of soot from diesel engines in trucks, in buses, in trains and in ships.

It is noted from Eq. (4) that the airflow rate can increase by restricting the decomposition rate. For example, the leftover concentration of toluene at the kerosene fuel rate of 1.87 kg/hr corresponding to E = 276.3 J/L in Fig. 2 is X_1/X_0 = 0.02 for R_1 = 5,000 lpm. Substituting these numbers into Eq. (4), we find that R_2 = 19,560 lpm for X_2/X_0 = 1/e. About 20,000 lpm of the contaminated air with toluene can be treated if the treatment is at a 63 percent elimination requirement.

As mentioned earlier, the compactness and lightweight of the decontamination system are critical issues for rapid mobility and quick installation in life threatening situations. The reaction chamber size used in the examples presented earlier is 22 cm diameter and 30 cm long, which limits the airflow rate. The linear dimension of the waveguide and discharge tube in the plasma torch system is proportional to the wavelength of microwaves. Therefore, the torch plasma volume is inversely proportional to the square of the microwave frequency. For example, the torch plasma volume increases 7 times by changing the microwave frequency from 2.45 GHz to 915 MHz with an additional power. The larger volume of the plasma flame in an increased reaction chamber with low-frequency microwaves and additional fuel means the more treatment of the airflow rate. The treatment volume can easily be enhanced by increasing the size of the plasma flame in an enlarged reaction chamber. Therefore, there will be no scientific problem to extend the treatment volume to 100,000 lpm, although the system size may increase accordingly.

4.2 Elimination of air contaminated with odorous chemical agents

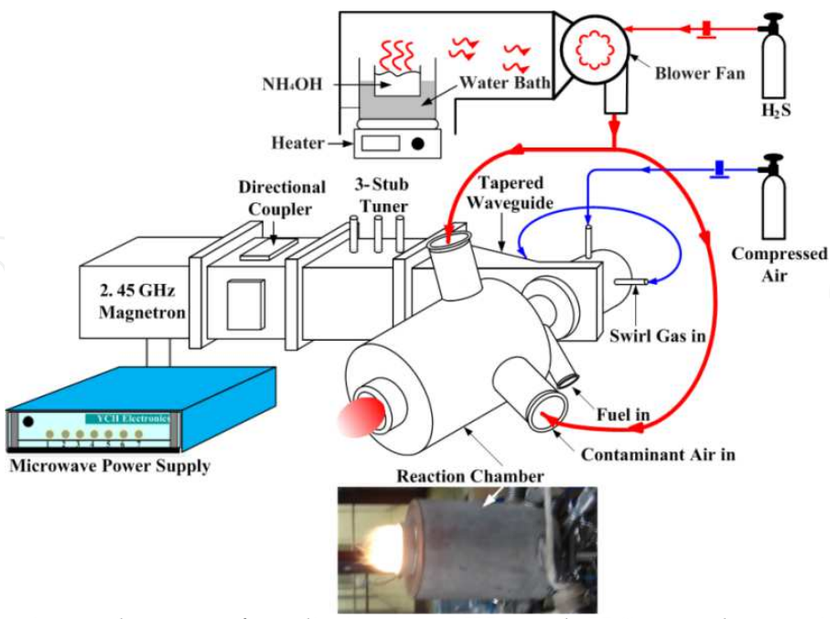

Fig. 14. Experimental set-up for eliminating NH_3 and H_2S as odor-causing chemical materials by making use of a microwave plasma burner. The inset is the picture of the kerosene plasma flame (Hong et al., 2007).

The inset in Fig. 14 shows the picture of the plasma flame produced from the microwave plasma burner at 1.4 kJ/s plasma power with no reflected power and 1.15 kg/hr kerosene. In Fig. 14, the blower fan connected to the reaction chamber by four stainless steel bellows sucks up air contaminated odorous gases, and transfers the contaminants into the reaction chamber. It can suck and blow airflow more than 5 000 litters per minute (lpm) at least. The reaction chamber consists of inner and outer compartment, providing a space between them. The contaminated air was injected into the reaction chamber via four injection ports in tangential direction installed on the outer compartment, thereby rotating in the space. In turn, the rotating airflows enter the inner compartment with tangential slits, which are also in tangential directions along the inner surface of the inner compartment wall, mixing with the plasma flame made of atmospheric microwave plasma and a fuel-burning flame. The dimensions of the reaction chamber used in the experiment were 22 cm diameter and 30 cm long. The plasma flame and the contaminated air in the inner compartment rotate in the same direction, providing the necessary residence time for the best elimination effects. These sequential processes then eliminate the odorous chemical agents in the passing air.

Aqua ammonia (NH_4OH) was used to obtain NH_3 gas in the simulated experiment for eliminating NH_3 and was maintained at 60 ˚C by a vaporization device in Fig. 14. On the other hand, in case of the simulated experiment of eliminating H_2S, gas-phase H_2S was directly injected into the blower fan and was mixed with air. The blower fan suck up air contaminated with NH_3 and H_2S gas, and transferred the contaminants into the reaction chamber. And then the total air-flow rate was approximately 5 000 lpm. 40 lpm of the compressed air as a swirl gas was injected into the microwave plasma torch. The injection rates of the kerosene were 1.15 kg/hr, 1.46 kg/hr and 1.87 kg/hr. The 1.15 kg/hr nozzle is the smallest fuel nozzle ever found. The methane flow rates were 5 lpm, 10 lpm, 15 lpm, 20 lpm and 30 lpm. The energy contained in kerosene and in methane are 10^7cal/kg and 9.52×10^6 cal/m^3, respectively. The fuel-flow rates injected can be translated into joules per second. The power of 1.15 kg/hr kerosene energy corresponds to 13.3 kJ/s and that of 20 lpm methane energy is also 13.3 kJ/s. The detailed simulated experiments for eliminating NH_3 and H_2S were carried out in terms of the input energy density of the microwave plasma burner. For instance, the kerosene injection rates of 1.15 kg/hr, 1.46 kg/hr, and 1.87 kg/hr with the 1.4 kJ/s plasma power correspond to the input energy densities 176.4 J/L, 219.4 J/L, and 276.3 J/L, respectively, for the total air-flow rate of 5 000 lpm.

In this work, the experimental results were presented by making use of a simple first order decay model for eliminating target chemicals. The destruction model (Hong et al., 2004) of the odorous chemicals can be expressed as $X/X_0 = \exp(-E/\beta)$, where X represents the leftover concentration of the odorous chemicals after the plasma flame treatment and X_0 is the initial concentration before the treatment, E denotes the input energy density (in units of joules per liter) deposited on the contaminated air by the plasma flame during the treatment and β represents the energy density required for bringing down the concentration to 1/e of its initial concentration; i.e. the energy density needed for 63 % destruction. The leftover concentrations of NH_3 and H_2S were measured by employing detector tubes from the GASTECH Company in Japan. The measurement by detector tubes was done at the flame exit of the reaction chamber without any delay or any interference. Therefore, the detector tube may reliably measure the leftover NH_3 and H_2S, although the data may have a large error bar. The data points in Fig. 15 indicate the average leftover NH_3 (open circle dots) and H_2S (open square dots) concentrations obtained from the repeated measurements in terms of

the input energy densities by means of the methane plasma burner. The closed square dots are the leftover H_2S concentrations by means of the kerosene plasma burner. The initial concentrations of NH_3 and H_2S was X_0 = 159 ppm and 120 ppm, respectively. The curves in Fig. 15 represent the least squared fits to the experimental data points for the microwave plasma burner. Eventually, the β-values of the NH_3 and H_2S elimination by the methane plasma burner are 39.69 J/L and 56.45 J/L, respectively. On the other hand, the β-value of H_2S elimination by the kerosene plasma burner is 46.52 J/L. The β-values of NH_3 and H_2S elimination by methane plasma burner are considerably less than 62.74 J/L for toluene and 138.02 J/L soot elimination, which were reported in the previous document (Uhm et al., 2006). In the recent article for decomposition of H_2S and NH_3 using a plate-to-wire pulse corona reactor (Huang et al., 2001), the β-values of H_2S (X_0 = 148 ppm) and NH_3 (X_0 = 58 ppm) decomposition were 65 J/L and 60 J/L, respectively. Gliding arc discharges (Dalaine et al., 1998; Czernichowski A. 1994) have been used as other example of H_2S depollution. Czernichowski (Czernichowski, 1994) reported that 7 Nm^3/h of air contaminated with 0.7% H_2S was completely purified at the energy consumption of 0.14 kWh per Nm^3 without any preheating. The energy in bringing down the concentration of its initial concentration to zero was estimated to be 540 J/L. In Fig. 15, the energy is approximately 300 J/L. Even though the initial concentrations are different for H_2S elimination, this work reveals that the kerosene microwave plasma burner may be more effective than the pulse corona reactor (Shi et al., 2005) and the gliding arc discharge (Czernichowski, 1994) in a standpoint of energy consumption. From the simple description for atomic oxygen produced in the microwave plasma burner (Hong & Uhm, 2006), the atomic oxygen density n_o was calculated to be n_o = $5.7 \times 10^{13}/cm^3$, which effectively combusts hydrocarbon fuels. It is also emphasized that a large volume of air can be treated by a compact apparatus in this study.

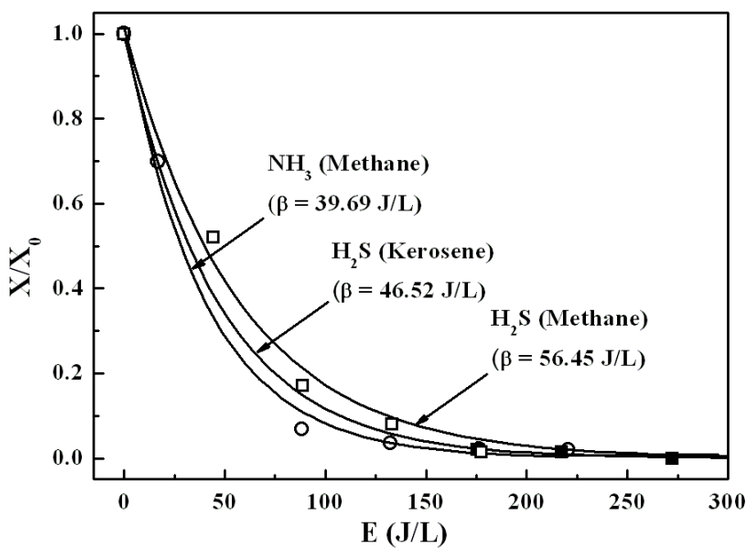

Fig. 15. Plots of leftover H_2S and NH_3 concentration in terms of the input energy density E. The closed and open square dots represent the data points of H_2S concentrations for kerosene and methane injection, respectively, and the open circle dots are NH_3 concentration data for methane injection. Each data point indicates the average value of eight repeated measurements (Hong et al., 2007).

4.3 Destruction of fluorinated compound gases

In NF_3 abatement, NF_3, N_2, O_2 and CH_4 were premixed in the gas-mixing vessel and injected from the side of the microwave plasma torch through FC and CH_4 gas injector. NF_3 can be directly ionized, attached, or dissociated to NF_x (x=0, 1, 2) radicals by electron impact processes, and the reaction is expressed as

$$NF_3 \rightarrow NF_x + F_y \quad (k = 6.6 \times 10^{-8} e^{(-24160/T)}\ \mathrm{cm^3/s}), \tag{5}$$

where y is 1 or 2, and T is gas temperature. The microwave plasma burner produces high-temperature, large-volume plasma flame (Hong et al., 2006). NF_3 gas is easily decomposed in high-temperature environment. For example, the reaction rate in Eq. (5) is 4.2×10^{-12} cm^3/s at 2500 K. In fact, average temperature of the methane plasma burner from the CH_4 injector to 20 cm away is approximately 2500 K (Bang et al., 2006). Therefore, abatement of FC gases using the methane microwave plasma burner is accomplished by both plasma and thermal decomposition. The chemical reactions described below are considered in a standpoint of the additive gas used for effective abatement, although there are many other possible reactions. When O_2 as an additive gas is used to abate NF_3, the desired reaction pathway of O_2 is to oxidize the nitrogen in NF_3 to N_xO_y. Whenever diatomic oxygen molecules meet electrons, they undergo dissociative attachment, which produces an O radical and O^- ion (Hong et al., 2003) for the electron temperature in the range of the present experiment. These oxygen atoms react with the NF_x radicals. The chemical reaction equations are

$$O + NF_2 \rightarrow NF + OF \quad (k = 10^{-12}\ \mathrm{cm^3/s}), \tag{6}$$
$$O + NF \rightarrow NO + F \quad (k = 10^{-12}\ \mathrm{cm^3/s}), \tag{7}$$
$$O + OF \rightarrow O_2 + F \quad (k = 5 \times 10^{-11}\ \mathrm{cm^3/s}). \tag{8}$$

Based on Eqs. (6)–(8), the final byproducts are nitrogen monoxide and fluorine at the downstream of the reactor. Also CH_4 electron impact dissociation produces H radicals. H radicals are precursors for FC remediation. As an example, the chemical reactions of NF_x by H radicals (Chang et al., 2000) are presented:

$$H + NF \rightarrow N + HF \quad (k = 1.5 \times 10^{-13}\ \mathrm{cm^3/s}), \tag{9}$$
$$H + F \rightarrow HF \quad (k = 1.6 \times 10^{-9}\ \mathrm{cm^3/s}). \tag{10}$$

As shown in Eqs. (9) and (10), the stable byproduct HF is formed by CH_4. It is well known that HF is water soluble and is easily captured by passing through a commercial wet scrubber. Although the plasma temperature decreases with the radius and the length of the plasma torch flame, NF_3 is easily decomposed to NF_x radicals with a high reaction rate at given temperatures, as shown Eq. (5). Therefore, we expect that all reactions presented in Eqs. (5) – (10) occur in the core of the plasma burner flame and HF contents increases in the afterglow.

In addition to NF_3 abatement, oxygen atoms also react with SF_x (x=1–5) radicals produced by electron impact processes, creating additional SO_2 or SO molecules and forming SOF_2 and SO_2F_2 molecules by F_2 reactions downstream of the plasma. The chemical reaction equations (Plumb & Ryan, 1988) are

$$O + SF_5 \rightarrow SOF_4 + F \quad (k = 2 \times 10^{-11}\ \mathrm{cm^3/s}), \tag{7}$$
$$O + SF_4 \rightarrow SOF_4 \quad (k = 2 \times 10^{-14}\ \mathrm{cm^3/s}), \tag{8}$$

$$O + SF_2 \rightarrow SOF_2 \quad (k = 1.08 \times 10^{-10}\ cm^3/s), \tag{9}$$
$$O + SF_4 \rightarrow SOF + F \quad (k = 7.63 \times 10^{-11}\ cm^3/s), \tag{10}$$
$$O + SF \rightarrow SOF \quad (k = 1.7 \times 10^{-10}\ cm^3/s), \tag{11}$$
$$O + SOF \rightarrow Products \quad (k = 7.9 \times 10^{-11}\ cm^3/s). \tag{12}$$

In the CF_4 abatement, the desired reaction pathway of O_2 is to oxidize the carbon in CF_4 to CO_2. When diatomic oxygen molecules meet electrons, they undergo dissociateve attachment that producing O radical and O^- ion at the electron temperature in this range of presented experiment. These oxygen atoms react with the CF_x radicals. The chemical reaction equations are (Hong et al., 2003)

$$O + CF_3 \rightarrow COF_2 + F \quad (k = 3.1 \times 10^{-11}\ cm^3/s), \tag{13}$$
$$O + CF_2 \rightarrow COF + F \quad (k = 1.4 \times 10^{-11}\ cm^3/s), \tag{14}$$
$$O + CF_2 \rightarrow CO + 2F \quad (k = 4.0 \times 10^{-11}\ cm^3/s), \tag{15}$$
$$O + CF \rightarrow CO + F \quad (k = 2.4 \times 10^{-11}\ cm^3/s). \tag{16}$$

The hydrogen radicals produced from the decomposition of CH_4 react with fluorine species and form simple, stable byproduct HF, as shown in Eq. (10).

As previously mentioned, FTIR was employed to identify the concentration changes of NF_3, SF_6, CF_4 and the plasma byproduct before and after the plasma burner treatment. The performance of the microwave plasma abatement device was described in terms of DRE. The DRE represents the percentage of FC gas that has been destroyed. In other words, the definition of DRE is

$$DRE\ (\%) = (S_{before} - S_{after}) / S_{before} \times 100, \tag{17}$$

where S_{before} and S_{after} are the main peak area of the FC gases before and after the plasma burner treatment, respectively.

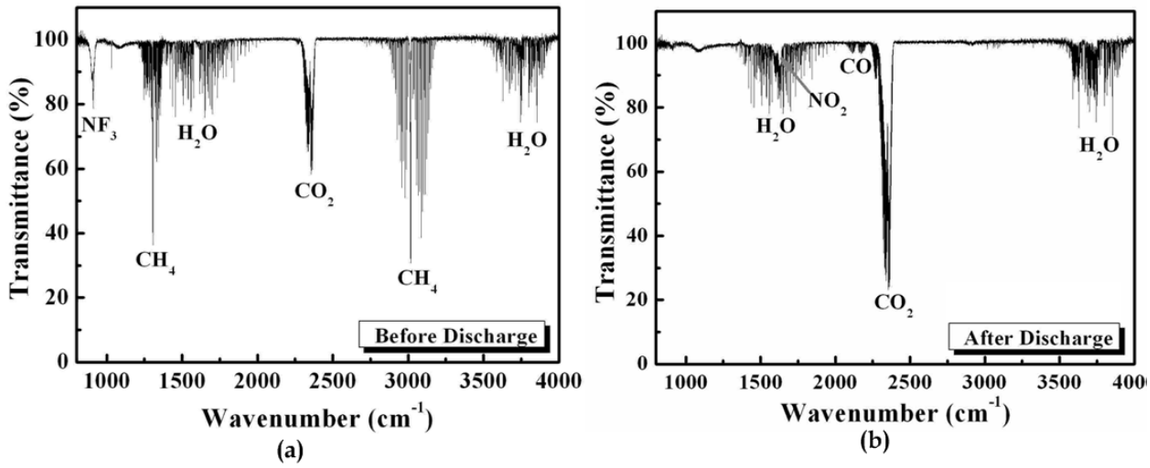

Fig. 16. FTIR spectra (a) before and (b) after the microwave plasma burner abatement of NF_3 with the components of 40 lpm compressed air as swirl gas, 250 lpm N_2, 30 lpm O_2, 15 lpm CH_4 and 0.6 lpm NF_3 at the applied plasma power of 1.2 kW (Hong et al., 2010).

Figures 16(a) and (b) show infrared transmitted spectra, demonstrating before and after the application of the microwave plasma burner to the components of 40 lpm swirl air, a mixture of 30 lpm O_2, 250 lpm N_2, 15 lpm CH_4 and 0.6 lpm NF_3 at the applied microwave power of 1.2 kW, respectively. The energy contained in the CH_4 is about 9.52×10^6 cal/m^3. The CH_4 injection rate can be translated into watt. For example, 15 lpm injection rate of methane is 9.98 kW. Therefore, total applied power is approximately 11.2 kW. As mentioned earlier, the microwave plasma torch showed a treatment limitation at high flow rates with low removal efficiency due to the drastic decrease of plasma volume and the short residence time of contaminants. The wavenumbers 910 and 1032 cm^{-1} on the horizontal line represent the signature of the NF_3 species. After the microwave plasma burner was turned on, the gas stream was analyzed. As expected, the CH_4 plasma burner destroyed almost all of the NF_3 contaminants with CH_4 decomposition rate close to 100%. The NO_2 curve in Fig. 16(b) represents the increases of the NO_2 molecules during the microwave discharge, because nitrogen in NF_3 is oxidized by O_2. Moreover, in air plasma, N_xO_y neutral molecules, $N_xO_y^-$ and $N_xO_y^+$ ions, will be formed, where NO_2 and N_2O, $N_2O_2^-$ and N_3O^+ are expected to be dominant neutral species, negative and positive ions, respectively. Therefore, NO_2 is formed. Generally, NO in the FITR spectrum is identified at 1950–1810 cm^{-1}. As shown in Fig. 16(b), the NO peak may be screened by strong H_2O peaks or the formation of NO may be minimal if there is any. HF can be formed through the reaction of F_2 with H_2O which may be in downstream of the plasma burner.

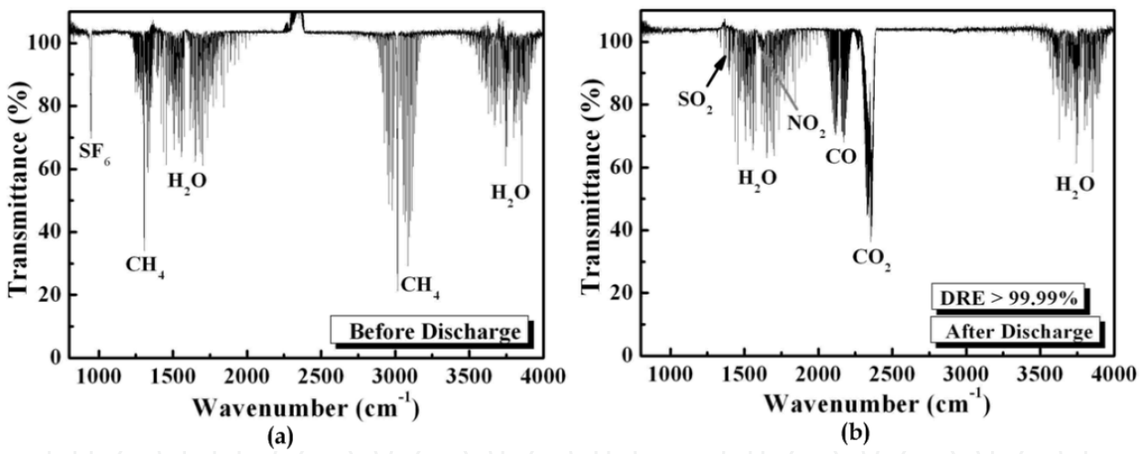

Fig. 17. FTIR spectra (a) before and (b) after the microwave plasma burner abatement of SF_6 with the components of 40 lpm compressed air as swirl gas, 120 lpm N_2, 30 lpm O_2, 15 lpm CH_4 and 0.1 lpm SF_6 at the microwave plasma power of 1.4 kW (Hong et al., 2010).

Figure 17 displays FTIR spectra before and after the application of the microwave plasma burner to the components of 40 lpm swirl air, a mixture of 30 lpm O_2, 120 lpm N_2, 15 lpm CH_4 and 0.1 lpm SF_6 at the applied microwave power of 1.4 kW. The translated total power for 15 lpm CH_4 is approximately 11.2 kW. The wavenumber 948 cm^{-1} on the horizontal line represents the signature of the SF_6 concentration, as shown Fig. 17(a). After the plasma burner treatment in Fig. 17(b), SF_6 concentration was significantly reduced, showing high DRE of 99.92%. SO_2 molecules at 1361 cm^{-1} as an important byproduct for decomposition of SF_6 were detected. The microwave plasma burner simultaneously destructed and burned

out the SF_6 contaminants by exothermic reactions with O_2 in compressed air injected as a swirl gas, forming HF molecules.

Figure 18 shows infrared transmitted spectra, demonstrating the microwave plasma burner abatement for CF_4. In the same experimental condition with the case of SF_6, a mixture of 40 lpm N_2 and 0.05 lpm CF_4 as contaminant was injected. In Fig. 18(a), the wavenumber 1283 cm^{-1} on the horizontal line represents the signature of the CF_4 concentration. In addition to NF_3 and SF_6, CF_4 was also abated in the experimental condition, showing 98.1% DRE in Fig. 18(b). Although the trace of CO and CO_2 as resultant products of CF_4 oxidation was not identified due to kerosene combustion, main byproducts are CO and CO_2.

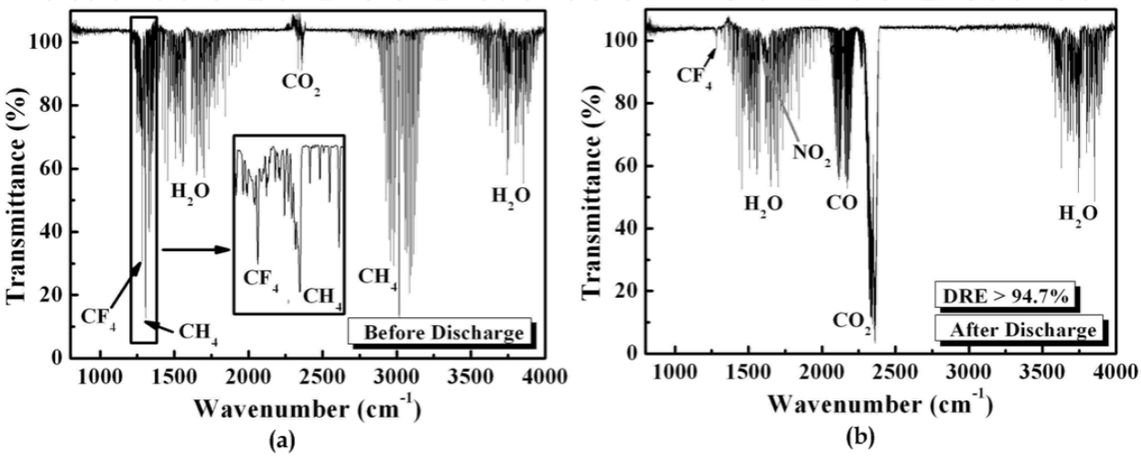

Fig. 18. FTIR spectra (a) before and (b) after the microwave plasma burner abatement of CF_4 (Hong et al., 2010).

Figure 19 shows the plot of the DREs of SF_6 and CF_4 versus nitrogen flow rates, corresponding to Figs. 17 and 18, respectively. The components of 40 lpm swirl air, a mixture of FC gas which is 0.1 lpm SF_6 or 0.05 lpm CF_4, 30 lpm O_2, 15 lpm CH_4 and various N_2 gas flow rates at the applied microwave power of 1.4 kW. DREs were measured in terms of N_2 flow rates. The N_2 flow rate of SF_6 and CF_4 abatement were from 40 lpm to 160 lpm and 20 lpm to 120 lpm, respectively. In case of SF_6 abatement, DREs were more than 99.9% until 120 lpm N_2, however, DREs of over 140 lpm N_2 were decreased drastically. At the N_2 flow rate over 140 lpm, plasma burner flame temperature, volume and residence time were decreased drastically. In this context, DRE of CF_4 was decreased drastically in terms of over 60 lpm N_2 flow. It is apparent that the abatement of CF_4 is much more difficult than that of SF_6. For instance, the DRE of SF_6 is more than 99.99% at 120 lpm N_2, while that of the CF_4 gas is only 46.2%. In particular, CF_4 has proven to be difficult to destroy and remove because of its chemical thermal stability due to the strong covalent nature of its bonding. Dissociation energies in SF_6 and CF_4 are represented by $e + SF_6 \rightarrow SF_5 + F + e$ (4.01 eV) and $e + CF_4 \rightarrow CF_3 + F + e$ (12.5 eV), respectively. The CF_4 dissociation energy is about three times of the SF_6 dissociation energy, which explains the observations in Fig. 19.

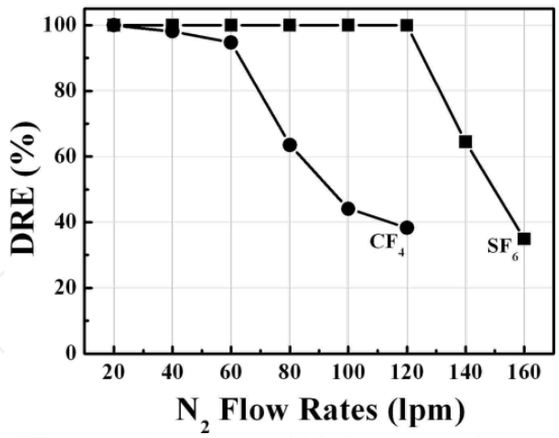

Fig. 19. DREs of SF_6 and CF_4 plotted in terms of N_2 flow rates (Hong et al., 2010).

Greenhouse gases that are subject to reduction under the Kyoto Protocol include HFCs, PFCs, SF_6, N_2), CH_4, and CO_2. Since the global warming potential (GWP) of the three fluorinated gas substitutes is several hundred to several tens of thousand times of that of CO_2, utmost efforts towards regulating their emission are required. In the present work, CO_2 emission from the combustion of 15 lpm CH_4 is about 29 grams per minute. And NF_3 emission from 0.5 lpm is about 1.5 grams per minute. GWP of NF_3 is very high as many as 9720 times in respect to CO_2. Therefore, we expect that CO_2 emission from the present plasma system is ignorable (Hong et al., 2010).

5. Conclusion

In order to significantly increase the volume and temperature of the microwave plasma torch, we have developed a microwave plasma-burner by injecting hydrocarbon fuel in liquid or gaseous state into the microwave plasma torch generated by air and a mixture of air and oxygen. The microwave plasma-burner implies that a plasma flame of high-power level can be obtained by only injecting small quantity of a hydrocarbon fuel. For example, the energy contained in diesel and in methane are approximately 10^7cal/kg and 9.52×10^6 cal/m^3, respectively. The fuel injection rate can be translated into watts. Eventually, a 0.019 lpm (≈ 1.15 kg/hr) injection rate of diesel is 13.3 kW and a 10 lpm CH_4 corresponds to approximately 6.6 kW. A significant temperature increase of the CH_4 microwave plasma burner was observed in relative to those of the microwave plasma torch and CH_4 fuel-only flame, showing the influence of the microwave plasma on the combustion flame.
In decontamination test of chemical agents, the plasma flame could be a very effective mean for decontaminating the airborne chemical and biological warfare agents. The plasma flame also provided a unique opportunity of a simultaneous elimination and burnout of chemical and biological warfare agents diluted in air. However, it is essential for the nations and their military, worldwide, to carry out the decontamination experiment of the real chemical and biological warfare agents for the experimental data, with which the plasma flame system makes the warfare agents obsolete. We also reported the experimental results for removing FC gases by using the methane microwave plasma burner and described the simple model for effective abatement of FC gases. In NF_3 abatement, we achieved a DRE of more than 99.9999% in the mixture of 0.6 lpm NF_3, 400 lpm N_2, 100 lpm O_2 and 15 lpm CH_4 by applying

the microwave power of 1.2 kW. In case of SF_6, we achieved a DRE of more than 99.9% in the mixture of 0.1 lpm SF_6, 120 lpm N_2, 30 lpm O_2 and 15 lpm CH_4 by at the applied microwave power of 1.4 kW. Also, DRE of CF_4 is 94.72% in the mixture of 0.05 lpm CF_4, 60 lpm N_2, 30 lpm O_2 and 15 lpm CH_4 at the microwave power of 1.4 kW. N_2 gas is required in post-pump systems. The aforementioned characteristics make the microwave plasma burner attractive for the destruction and removal of chemically stable gases emitted by the semiconductor industry.

6. References

Bang, C.U., Hong, Y.C., Cho, S.C., Uhm, H.S. & Yi, W.J. (2006): Methane-Augmented Microwave Plasma Burner, *IEEE Trans. Plasma Sci.* Vol. 34, No. 5, pp 1751-1756, ISSN 0093-3813.

Chang, J.-S., Urashima, K.G., Yamamoto, K., Okayasu, T., Kato, Y., Iwaizumi, T. & Yoshimura, K. (2000): Removal of NF_3 from semiconductor-process flue gases by tandem packed-bed plasma and adsorbent hybrid systems, *IEEE Trans. Ind. Appl*. Vol. 36, No. 5, pp 1251-1259, ISSN 0093-9994.

Czernichowski, A. (1994): Gliding arc: applications to engineering and environment control, *Pure Appl. Chem*. Vol. 66, No. 6, pp 1301-1310, ISSN 1365-3075.

Delaine, V., Cormier, J.M, Pellerin, S. and Lefaucheux, P. (1998): H_2S destruction in 50 hz and 25 kHz gliding arc reactor, *J. App. Phys.* Vol. 84, No. 3, pp 1215-1221, ISSN .

de Izarra, C. (2000): Computer simulation of the UV OH band spectrum, *Int. J. Mod. Phys. C* Vol. 11, No. 5, pp 987-998, ISSN 1793-6586.

Hartz, C.L., Bevan, J.W., Jackson, M.W. & Wofford, B.A. (1998): Innovative surface wave plasma reactor technique for PFC abatement, *Environ. Sci. Technol*. Vol. 32, No. 5, pp 682-687, ISSN 0013-936X.

Fauchais, P. & Vardelle, A. (1997): Thermal plasmas, *IEEE Trans. Plasma Sci.* Vol. 25, No. 6, pp 1258-1280, ISSN 0093-3813.

Green, K.M., Borass, M.C., Woskov, P.P., Flores, G.J., Haddi, K. & Thomas, P. (2001): Electronic excitation temperature profiles in an air microwave plasma torch, *IEEE Trans. Plasma Sci.* Vol. 29, No. 2, pp 399-406, ISSN 0093-3813.

Gutsol, A. & Bakken, J.A. (1998): A new vortex method of plasma insulation and explanation of the Ranque effect, *J. Phys. D: Appl. Phys.* Vol. 31, No. 6, pp 704-708, ISSN 1361-6463.

Hong, Y.C., Kim, J.H. & Uhm, H.S. (2003): Abatement of CF_4 by atmospheric pressure microwave plasma torch, *Phys. Plasmas* Vol. 10, No. 8, pp 3410-3414, ISSN 1089-7646.

Hong, Y.C., Kim, J.H. & Uhm, H.S. (2004): Simulated experiment for elimination of chemical and biological warfare agents by making use of microwave plasma torch, *Phys. Plasmas* Vol. 11, No. 2, pp 830-835, ISSN 1089-7646.

Hong, Y.C., Uhm, H.S., Kim, H.S., Kim, M.J., Han, S.H., Ko, S.C. & Park, S.K. (2005): Decomposition of phosgene by microwave plasma-torch generated at atmospheric pressure, *IEEE Trans. Plasma Sci.* Vol. 33, No. 2, pp 958-963, ISSN 0093-3813.

Hong, Y.C., Cho, S.C., Bang, C.U., Shin, D.H., Kim, J.H., Uhm, H.S. & Yi, W.J. (2006): Microwave plasma burner and temperature measurements in its flame, *Appl. Phys. Lett.* Vol. 88, No. 20, pp 201502-201504, ISSN 0003-6951.

Hong, Y.C., Shin, D.H. & Uhm, H.S. (2007): Simulated experiment for elimination of air contaminated with odorous chemical agents by microwave plasma burner, *Appl. Phys. Lett*. Vol. 91, No. 16, pp 161502-161504, ISSN 0003-6951.

Hong, Y.C., Lho, T., Shin, D.H. & Uhm, H.S. (2010): Removal of fluorinated compound gases by an enhanced methane microwave plasma burner, *Jpn. J. Appl. Phys.* Vol. 49, No. 1, pp 017101-017106, ISSN 1347-4065.

Huang, L., Nakajo, K., Ozawa, S. & Matsuda, H. (2001): Decomposition of dichloromethane in a wire-in-tube pulsed corona reactor, *Environ. Sci. Technol*. Vol. 35, No. 6, pp 1276-1281, ISSN 0013-936X.

Kim, J.H., Hong, Y.C., Kim, H.S. & Uhm, H.S. (2003): Simple microwave plasma source at atmospheric pressure, *J. Korean Phys. Soc.* Vol. 42, No. 92, pp S876-S879, ISSN 1976-8524.

Kim, J.H., Hong, Y.C. & Uhm, H.S. (2007): Binary oxide material made from a mixture of Zn and Cd in a microwave plasma, *Chem. Phys. Lett*. Vol. 443, No. 1, pp 122-126, ISSN 0009-2614.

Lai, W., Lai, H., Kuo, S.P., Tarasenko, O. & Levon, K. (2005): Decontamination of biological warfare agents by a microwave plasma torch, *Phys. Plasmas* Vol. 12, No. 5, pp 023501-023506, ISSN 1089-7646.

Margot, J. (2001): Studies of emission spectra in helium plasmas at atmospheric pressure and local thermodynamical equilibrium, *Phys. Plasmas* Vol. 8, No. 5, pp 2525-2532, ISSN 1089-7646.

Masuya, G., Takita, K., Takahashi, K., Takatori, F. & Ohzeki, H. (2002): Effects of airstream mach number on H/N plasma igniter, *J. Propul. Power* Vol. 18, No. 3, pp 679-685, ISSN 0748-4658.

Moisan, M., Zakrzewski, Z. & Rostaing, J.C. (2001): Waveguide-based single and multiple nozzle plasma torches: the TIAGO concept, *Plasma Sources Sci. Technol.* Vol. 10, No. 3, pp 387-394, ISSN 1361-6595.

Moon, S.Y., Choe, W., Uhm, H.S., Hwang, Y.S. & Choi, J.J. (2002): Characteristics of an atmospheric microwave-induced plasma generated in ambient air by an argon discharge excited in an open-ended dielectric discharge tube, *Phys. Plasmas* Vol. 9, No. 9, pp 4045-4051, ISSN 1089-7646.

Ogawa, S., Sakai, Y., Sato, K. & Sega, S. (1998): Influence of microwave on methane-air laminar flames, *Jpn. J. Appl. Phys.* Vol. 37, No. 1, pp 179-185, ISSN 1347-4065.

Penetrante, B.M., Hsiao, M.C., Merritt, B.T., Vogtlin, G.E., Kuthi, A., Burkhart, C.P. & Bayless, J.R. (1997): Identification of mechanisms for decomposition of air pollutants by non-thermal plasma processing, *Plasma Sources Sci. Technol.* Vol. 6, No. 3, pp 251-2598, ISSN 1361-6595.

Plumb, I.C. & Ryan, K.R. (1998): Gas-phase reactions in plasmas of SF_6 with O_2: Reactions of F with SOF_2 and SO_2 and rections of O with SOF_2, *Plasma Chem. Plasma Prccess.* Vol. 9, No. 3, pp 409-420, ISSN 0272-4324.

Shi, Y., Ruan, J., Wang, X., Li, W. & Tan, T. (2005): Decomposition of mixed maldorants in a wire-plate pulse corona reactor, *Environ. Sci. Technol*. Vol. 39, No. 17, pp 6786-6791, ISSN 0013-936X.

Takita, K., Masuya G., Sato T. & Ju, Y. (2001): Effect of addition of radicals on burning velocity, *AIAA J.* Vol. 39, No. 4, pp 742-744, ISSN 0001-1452.

Uhm, H.S. (1999): Properties of plasma flames generated by electrical breakdown in flames, *Phys. Plasmas* Vol. 6, No. 11, pp 4366-4674, ISSN 1089-7646.

Uhm, H.S., Hong, Y.C. & Shin, D.H. (2006): Plasma flame for mass purification of contaminated air with chemical and biological warfare agents, *Appl. Phys. Lett*. Vol. 89, No. 12, pp 121504-121506, ISSN 0003-6951.

Weinberg, F.J., Hom, K., Oppenheim, A.K. & Teichman, K. (1978): Ignition by plasma jet, *Nature* Vol. 272, No. 5651, pp 341-343, ISSN 0028-0836.

Woskov, P.P. & Haddi, K. (2002): Large electrodeless plasmas at atmospheric pressure sustained by a microwave guide, *IEEE Trans Plasma Sci*. Vol. 30, No. 1, pp 156-157, ISSN 0093-3813.

IntechOpen

Fuel Injection

Edited by Daniela Siano

ISBN 978-953-307-116-9
Hard cover, 254 pages
Publisher Sciyo
Published online 17, August, 2010
Published in print edition August, 2010

Fuel Injection is a key process characterizing the combustion development within Internal Combustion Engines (ICEs) and in many other industrial applications. State of the art in the research and development of modern fuel injection systems are presented in this book. It consists of 12 chapters focused on both numerical and experimental techniques, allowing its proper design and optimization.

INTECH
open science | open minds

InTech Europe
University Campus STeP Ri
Slavka Krautzeka 83/A
51000 Rijeka, Croatia
Phone: +385 (51) 770 447
Fax: +385 (51) 686 166
www.intechopen.com

InTech China
Unit 405, Office Block, Hotel Equatorial Shanghai
No.65, Yan An Road (West), Shanghai, 200040, China
中国上海市延安西路65号上海国际贵都大饭店办公楼405单元
Phone: +86-21-62489820
Fax: +86-21-62489821

IntechOpen